Hindawi
Journal of Nanomaterials
Volume 2022, Article ID 7398110, 14 pages
https://doi.org/10.1155/2022/7398110

Research Article

Thermal Management of the Melting Process in a Latent Heat Triplex Tube Storage System Using Different Configurations of Frustum Tubes

Mohammadreza Ebrahimnataj Tiji,[1] Waleed Khalid Al-Azzawi,[2] Hayder I. Mohammed,[3] Anmar Dulaimi,[4] Farhan Lafta Rashid,[5] Jasim M. Mahdi,[6] Hasan Sh. Majdi,[7] Pouyan Talebizadehsardari,[8] and Hafiz Muhammad Ali[9,10]

[1]*Department of Mechanical Engineering, Qom University of Technology, Qom, Iran*
[2]*Department of Medical Instrumentation Engineering Techniques, Al-Farahidi University, Baghdad 10015, Iraq*
[3]*Department of Physics, College of Education, University of Garmian, Kurdistan, Kalar 46021, Iraq*
[4]*College of Engineering, University of Warith Al-Anbiyaa, Karbala 56001, Iraq*
[5]*Petroleum Engineering Department, College of Engineering, University of Kerbala, Karbala 56001, Iraq*
[6]*Department of Energy Engineering, University of Baghdad, Baghdad 10071, Iraq*
[7]*Department of Chemical Engineering and Petroleum Industries, Al-Mustaqbal University College, Babylon 51001, Iraq*
[8]*Centre for Sustainable Energy use in Food Chains, Institute of Energy Futures, Brunel University London, Kingston Lane, Uxbridge, Middlesex UB8 3PH, UK*
[9]*Mechanical Engineering Department, King Fahd University of Petroleum and Minerals, Dhahran 31261, Saudi Arabia*
[10]*Interdisciplinary Research Center for Renewable Energy and Power Systems (IRC-REPS), King Fahd University of Petroleum and Minerals, Dhahran 31261, Saudi Arabia*

Correspondence should be addressed to Pouyan Talebizadehsardari; pouyan.talebizadehsardari@brunel.ac.uk and Hafiz Muhammad Ali; hafiz.ali@kfupm.edu.sa

Received 21 March 2022; Revised 9 June 2022; Accepted 5 July 2022; Published 4 August 2022

Academic Editor: Hui Yao

In this study, the energy charging mechanism is mathematically modeled to determine the impact of design modifications on the thermofluidic behavior of a phase change material (PCM) filled in a triplex tube containment geometry. The surface area of the middle tube, where the PCM is placed, is supported by single or multi-internal frustum tubes in vertical triplex tubes to increase the performance of the heating and cooling of the system. In addition to the ordinary straight triplex tubes, three more scenarios are considered: (1) changing the middle tube to the frustum tube, (2) changing the inner tube to the frustum tube, and (3) changing both the internal and central tubes to the frustum tubes. The impact of adopting the tube designs and gap width were studied. The outcomes reveal that the heat storage rates are increased for all frustum tube systems compared to the straight tube system. According to the results, the case of a gap width of 5 mm is the optimal one among the studied cases in terms of the melting time and the heat storage rate. Employing the frustum tube configuration with a 5-mm gap width would save the melting time by 25.6% and increase the rate of heat storage by 32.8% compared to the base case of straight tubes.

1. Introduction

Saving global energy resources requires efficient conversion methods and consistent renewable energy sources [1, 2]. Almost 1/3 of the worldwide energy supply is wasted because of ineffective energy conversion techniques, harming the environment [3, 4]. Some renewable energy sources like wind, geothermal, and solar thermal energies suffer from erratically power supply, which creates a significant imbalance between the production and consumption of energy

[5–7]. Thermal energy storage (TES) system is a promising technique to cover the gap; for instance, a thermal storage system can store energy from the sun throughout the day and utilize it during the night or when the demand is high [8–10]. TES is classified into three modes: sensible heat, latent heat, and thermochemical storage. The primary purpose of TES mechanisms is to lower the energy loss and the cost to permit the manufacture of well cost-efficient energy conversion units [11, 12]. Phase change materials (PCMs) are considered one category of the most encouraging materials to store and recover the thermal energy in demand [13, 14].

Recently, the research interest regarding latent heat thermal energy storage (LHTES) increased due to the high thermal efficiency and low phase change temperature point; however, the thermal conductivity of the PCM is generally poor and inappropriate for many applications [15–17]. Accordingly, various techniques have been modelled to improve the heat transfer efficiency of the PCM during the charging and discharging methods [18]. These techniques include a combination with the high conductive materials (nanoparticles) [19–23], utilizing an extended surface area for the heat transfer (fins) [21, 24–26], combinations with the metal foam [27–31], and using more efficient geometries designs [28, 32, 33]. Moreover, natural convection is a critical mechanism that can assist the phase change heat transfer in molten regions. The magnetic field can influence natural convection heat transfer in molten regions of a PCM [34] and viscosity alteration [35].

Many investigations have been achieved to improve the thermofluidic behavior during the PCM's melting and solidification processes, which saves the required time for these operations [36, 37]. Various geometrical aspects have been considered for the LHTES system regarding the design and the shape of the heat transfer fluid (HTF), number of the channels, their positions, and distributions [38]. Park et al. [39] numerically studied the melting process of the PCM in a multichannel HEX LHTES. The impact of the channel number and design on the melting performance of the PCM was investigated regarding thermal management, provided power, and charging period. They found that the melting rate increases by increasing the number of the channels in the early stage, whereas the volumetric energy increases by 18.2% using eight HTF channels compared to a single large channel. Kousha et al. [40] experimentally examined the influences of utilizing different numbers and locations of the HTF channels on the phase change processes of the PCM at various temperatures of the inlet HTF (water). They found that the phase change time reduces using multi-HTF channels compared with the case of a single channel. They also found that increasing the inlet temperature to 80 °C accelerates the charging and the discharging rate by 43% and 50%, respectively. Talebizadehsardari et al. [41] studied the effect of various designs and the number of HTF channels utilizing a serpentine tube. They found that the discharging time and the output temperature of the HTF in the case of the serpentine tube were 6 hours and 56 °C compared with the straight tube, which was 13.6 hours and 41 °C. Mohammed [42] studied the discharge improvement of a phase change material-air-based thermal energy storage unit for space heating applications using metal foams in the air sides. The results showed that the HTF flow rate has a great influence on the discharging rate. The presence of the porous medium in the system improves the discharging process by 116% compared with a non-porous medium system at the same flow rate.

Heat exchangers (HEX) significantly impact manufacturing and engineering functions [43, 44]. Because of limited energy sources and cost considerations, more attention has been paid to improving the performance of the HEX [45, 46]. Thus, there is a significant demand to improve the thermal efficiency of the HEX, which managed to be employing and emerging various enhancement methods [47, 48]. The most common HEX utilized in the factories is shell and tube heat exchanger (STHE). A standard STHE contains a cylindrical shell, including many channels. Pourakabara and Darzi [49] performed a numerical model to predict the charging and discharging processes using different numbers of HTF tubes in the cylindrical and elliptical shapes of the shell embedded in the metal foam. They found that the peaks of the charging and discharging rates achieve 92% and 94%, respectively, when the porous medium is used compared with the system of alone PCM. Likely, Qaiser et al. [50] performed a numerical and experimental study by applying multi-finned channels with various designs of shell form (circular, elliptical, and rectangular). The thermal rate improved by 34% and 24%, and the charging rate was increased by 28% and 22% when utilizing two-vertical channels and v-array triple-channel design, respectively, in the circular shell of the LHTES system as compared to those in the reference case. Yang et al. [51] studied the Design of non-uniformly distributed annular fins for a shell-and-tube thermal energy storage unit. They found that moving fins down effectively improves the melting fraction of middle and bottom PCMs. Also, they detected that an 84.7% improvement in melting uniformity was achieved by a non-uniform design. Guo et al. [52] studied the compression effect of metal foam on melting phase change in a shell-and-tube unit. Yang et al. [53] investigated the effect of fin number on the melting phase change in a horizontal finned shell-and-tube thermal energy storage unit, and they found that the melting time can maximally be saved as high as 72.85% by increasing fin number. Guo et al. [54] examined the thermal assessment of a solid-liquid energy storage tube packed with non-uniform angled fins. In a different work, Guo et al. [55] studied the melting assessment on the angled fin design for a novel latent heat thermal energy storage tube, and they stated that the angled fins with small angles (5°, 10°, and 15°) markedly reduced full melting time for the TES unit. Eisapour et al. [56] optimized the configuration of a double elliptical LHTES through the charging process. They found that the efficiency of the system increases as the gap between the inner channel and the lower wall of the external channel reduces. The best place was located when the internal channel is at the minimum distance of the elliptical wall by 2 mm. Ren et al. [57] investigated the efficiency of shell-and-tube PCM in TES. They found that the spiral tube design and the double serpentine

tube design mostly have an advantage over the single serpentine tube design. The melting duration 95% of the PCM decreased by 16% if the single serpentine design was replaced to spiral (at the tube length of 4055 mm). Further, Patel et al. [58, 59] investigated the impact of the longitudinal fin inside the triplex tube in two different studies, and they found that each parameter related to the fins, including the arrangement, length, width and the number, has a great impact on the thermal performance of the heat storage unit.

Alnakeeb et al. [60] modeled the thermal parameters of the charging process influenced by a single planed tube with various inside eccentricities (0, 0.25, 0.5, and 0.75) and aspect ratios (0.5, 0.6, 0.7, 0.8, 0.9, and 1). The highest charging rate was found at 218.5% for the circular tube (aspect ratio of 1). Zheng et al. [61] examined the impact of internal circular tube eccentricity and Rayleigh number (Re) on phase change material melting and solidification heat transfer. They found that the highest eccentricity in the internal channel to the shell bottom did not necessarily offer the fastest melting rate. The best eccentricity was detected to have a linear relation with Re. The growth in the eccentricity increased the discharging rate just when the Re ratio (Re of discharging divided by charging) was greater than 2.0. Pahamli et al. [62] performed a numerical analysis to examine the impact of eccentricity, velocity, and inlet temperature of heat transfer fluid (HTF) on PCM charging characteristics. Raising the eccentricity from 0 to 0.75 increased the charging rate by 64% and 27%, respectively; simultaneously, the velocity had a minimal effect on the charging rate. Faghani et al. [63] modelled the behavior of the PCM charging in a variety of internal and exterior channel configurations, including vertical, horizontal, and circular ellipses. The shell's horizontal ellipse configuration and the channel's vertical ellipse demonstrated the maximum charging rate. Faghani et al. [63] modeled the operation of PCM charging by utilizing various designs of internal and external channels (circular, horizontal, and vertical ellipses). The arrangement of the horizontal ellipse form of the shell and the vertical ellipse form of the channel showed the highest charging rate. Gorzin et al. [64] conducted a model to examine the impact of various multi-tube LHTES system formations and PCM mass allocations on the discharging rate at different concentrations of nanoparticles. The appropriate allocation of PCM volume increases the discharging rate by 62%, while increasing the loading of the nanoparticles to 4 wt% reduces the discharging time by 15%.

The studies in the literature confirmed that the phase change process of PCM in TES systems is highly influenced by the number of HTF tubes and their geometries, which influence the melting rate and the required duration to complete one cycle. Therefore, a comprehensive investigation has been performed, including studying the angle of the PCM shell. Instead of three circular tubes, a combination of cone and frustum tubes has been utilized in the TES, which may improve the heat transfer in the system through the melting process. Thus, the current study aims to achieve the fastest melting rate and the best thermal performance at the specific distance between the internal and external channels (middle tube hydraulic diameter). The simulation of the melting processes in the different cases was achieved using ANSYS-Fluent software. Eventually, to improve the performance of the novel combination of cone and frustum tube latent heat thermal energy storage, sensitivity analysis of the solidification process could be achieved with the same procedures as the melting process.

2. Problem Description

A vertical triplex tube is examined as a latent heat TES in this study. The surface area of the middle tube, where the PCM is placed, is supported by single or multi-internal frustum tubes to increase the rate of heat transfer during the melting process. In the heat exchanger, the inner and outer tubes pass the heat transfer fluid (HTF), considered water in this study. The HTF flows in the opposite direction in both the internal and the external channels. The direction of the flow is affecting on temperature differences. The maximum temperature is shown at the inlet section and the minimum at the outlet section. The temperature differences directly affect the heat transfer by convection and conduction as well. The height of the tube is considered 250 mm. In the system with straight tubes, the hydraulic diameters of the inner, middle, and outer tubes are considered 20 mm, and the thickness of the inner and outer tubes is also considered 1 mm. It should be noted that the dimensions of the base system are chosen based on the triplex tube latent heat storage systems in the literature [65, 66]. In addition to the ordinary straight triplex tubes shown in Figure 1(a), there are three more scenarios considered in this study, including changing the middle tube to a frustum tube (Figure 1(b)), changing the inner tube to a frustum tube (Figure 1(c)), and changing both the inner and middle tube to frustum tubes (Figure 1(d)). In addition to the various tube designs, different gap widths are assessed considering the hydraulic diameters of 5, 10, and 15 mm for the middle tube at the bottom of the heat exchanger. The hydraulic diameter of the middle tube at the top of the heat exchanger is then determined considering a constant volume for the PCM equal to the PCM volume in the straight triplex tube heat exchanger. It should be noted that in scenario 2 (changing the inner tube to frustum tube), it is not possible to use 5 mm as the hydraulic diameter of the pipe at the bottom due to the slope of the frustum and dimensions of the system.

Because of the nature of the heat transfer issue being examined and the scarcity of circumferential flow difference, the unit is regarded as axisymmetric, as seen in Figure 2. The boundary conditions and directions of the HTF flow, and gravity, are also illustrated in Figure 2.

Table 1 presents the width of the PCM channel at the bottom of the heat exchanger for different proposed scenarios. As mentioned, the widths of the PCM at the top and HTF channels at the bottom and top are then determined according to the volume of the PCM compared with the base case (straight pipes).

Paraffin RT-35 is used as the PCM, whose thermophysical characteristics are listed in Table 2. The HTF's input temperature and flow Reynolds number are set to 50 °C

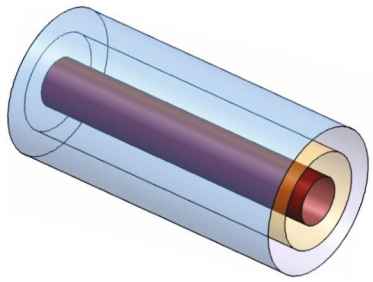

(a) Base case: straight tubes with no tube geometry modification

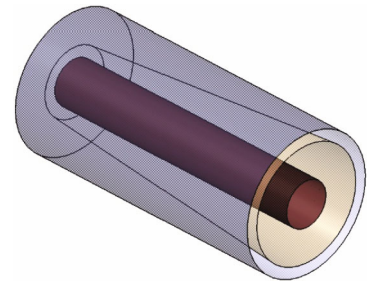

(b) Scenario 1: changing the middle tube to the frustum

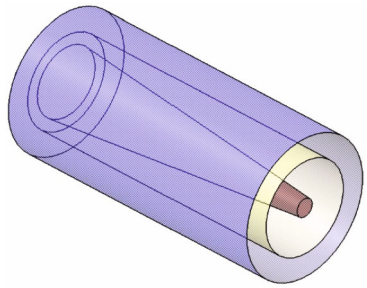

(c) Scenario 2: changing the inner tube to the frustum

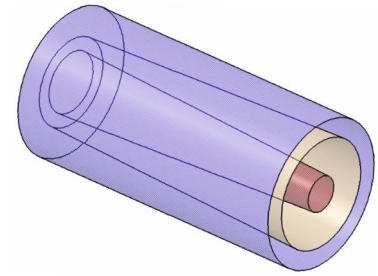

(d) Scenario 3: changing both the inner and middle tube to the frustum

Figure 1: The schematic of the vertical triplex tube TES system with different tube geometry modifications.

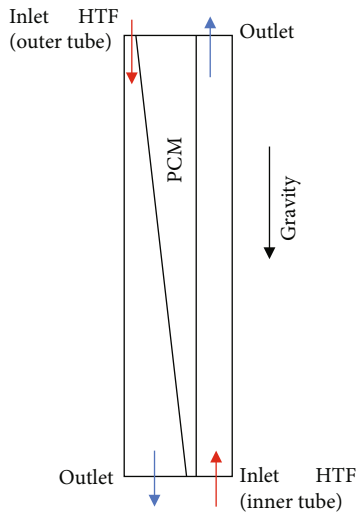

Figure 2: A schematic of the studied triplex tube in axisymmetric condition.

and 1000, respectively, to determine the optimal design. The PCM's initial temperature is regarded to be 15 °C.

3. Mathematical Modeling

In order to simulate the phase change of PCM, the enthalpy-porosity approach developed by Brent et al. [67, 68] was implemented. In this method, the liquid part and the porosity were presumed to be the same in all cells of the computational domain. To simplify the numerical solution of the governing differential equations, the following assumptions are considered as follows:

(i) Utilizing the Boussinesq approximation to control the density and buoyant force.

(ii) The fluid flow of molten PCM is transient, laminar, and incompressible.

(iii) Gravitation acceleration is positive in the – (Ve) y -axis direction.

(iv) The Boussinesq approximation is applicable to control the density and buoyant force.

(v) Perfect insulations are considered at the external boundaries.

(vi) The no velocity-slip condition is applied at the solid boundaries.

For the HTF and the molten PCM, the continuity, momentum, and energy are then defined as follows [8]:

$$\frac{\partial \rho}{\partial t} + \nabla . \rho \vec{V} = 0, \tag{1}$$

$$\rho \frac{\partial \vec{V}}{\partial t} + \rho\left(\vec{V}.\nabla\right)\vec{V} = -\nabla P + \mu\left(\nabla^2 \vec{V}\right) - \rho\beta\left(T - T_{ref}\right)\vec{g} - \vec{S}, \tag{2}$$

$$\frac{\rho C_p \partial T}{\partial t} + \nabla\left(\rho C_p \vec{V} T\right) = \nabla(k\nabla T) - S_L, \tag{3}$$

The factor $(\vec{S})$ in the momentum formula is involved to measure the impact of phase change, which is identified as

Table 1: The dimensions of the PCM width at the bottom of the heat exchanger in various studied scenarios for various cases.

Base case	Scenario 1		Scenario 2		Scenario 3			
Case 0 $\delta = 20$ mm	Case 1 $\delta = 5$ mm	Case 2: $\delta = 10$ mm	Case 3: $\delta = 15$ mm	Case 4: $\delta = 10$ mm	Case 5: $\delta = 15$ mm	Case 6: $\delta = 5$ mm	Case 7: $\delta = 10$ mm	Case 8: $\delta = 15$ mm

Table 2: Thermodynamic properties of the utilized PCM [35].

Properties	ρl [kg/m^3]	ρs [kg/m^3]	L_f [kJ/kg]	C_p [kJ/kg.K]	K [W/m.K]	μ [N.s/m^2]	T_L [°C]	T_S [°C]	β [J/K]
Values	770	860	170	2	0.2	0.023	36	29	0.0006

Table 3: Effect of grid size and time step size on the charging time.

Number of cells	28500		43000		81620
Time step size (s)	0.2	0.1	0.2	0.4	0.2
Melting time	4644	4733	4727	4701	4739

the velocity inhibiting term in Darcy law [69] :

$$\vec{S} = A_m \frac{(1-\lambda)^2}{\lambda^3 + 0.001} \vec{V} \tag{4}$$

The parameter of the mushy zone A_m is taken as 10^5 based on the literature [68, 70]. To evaluate the phase transition progression, λ (liquid part of PCM) is announced as follows [71]:

$$\lambda = \frac{\Delta H}{L_f} = \begin{Bmatrix} 0 & \text{if } T < T_S \\ 1 & \text{if } T > T_L \\ \dfrac{T - T_S}{T_L - T_S} & \text{if } T_S < T < T_L \end{Bmatrix} \tag{5}$$

The Boussinesq approximation is used to calculate the density variations because of the temperature variation through the PCM's phase change course. In this calculation, mass density is treated as fix value, excluding in the gravity term of the momentum formula, where density is observed as a temperature-dependent variable [72]:

$$\rho = \rho_{ref}\left(1 - \beta\left(T - T_{ref}\right)\right) \tag{6}$$

In the above equation, the reference temperature is the melting point (Tl + Ts/2), and the density is calculated at the reference temperature which is the average density of the PCM at the liquid and solid states. Then, the buoyancy effect is calculated for the temperatures higher than the melting temperature.

The source term S_L in the energy formula is found as

$$S_L = \frac{\rho \partial \lambda L_f}{\partial t} + \rho \nabla\left(\vec{V} \lambda L_f\right). \tag{7}$$

The rate of energy stored through the charging progression is calculated as

$$\dot{E_T} = \frac{E_{end} - E_{ini}}{t_m}, \tag{8}$$

where t_m is the charging time and E_e and E_i are the whole PCM's energy at the start and the endpoints of the charging progress. E is the total heat the sensible $(MC_p dT)$ and latent (ML_f) cases of the PCM.

4. Numerical Modeling, Grid Analysis, and Validation

A combination of the SIMPLE algorithm for pressure-velocity coupling and the Green-Gauss cell-based approach was utilized within the ANSYS-FLUENT solver to assess the heat transfer and fluid flow governing equations of PCM through the phase transition progress. For the momentum and energy equations, the QUICK differencing technique was utilized with the PRESTO scheme for the pressure correction equations. The under-relaxation factors are adopted after careful selection as 0.3, 0.3, 0.5, and 1 for pressure correction, velocity components, liquid fraction, and energy equation, respectively. The convergence criteria for terminating the iterative solution are set to be 10^{-4}, 10^{-4}, and 10^{-6} for the continuity, momentum, and energy equations, respectively.

The mesh and the time step size independency tests are performed. Accordingly, the various grid size of 28500, 43000, and 81620 are assessed utilizing the time step size of 0.2 s for the straight triplex system. Table 3 presents the melting time for various mesh densities. As illustrated, the outcomes are almost the same for the cell numbers 43000 and 81620; the mesh size of 43000 is selected for the next steps of this study. Table 3 also presents the melting time for various sizes of time step sizes for the nominated cell number. As demonstrated, the outcomes data are virtually identical for the time step of 0.1, 0.2, and 0.4 s, especially for the values 0.2 and 0.1 s. Thus, 0.2 s is selected as the time step size in the current work.

To verify the appropriateness of the simulation model describe above, the outcomes of Mat et al. [71] were utilized

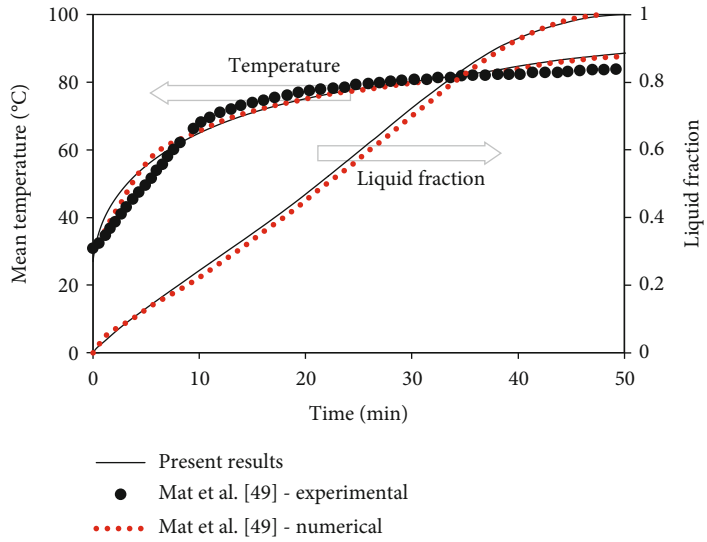

Figure 3: Evaluation of the current model's temperature and liquid-fraction results compared to those of Mat et al. [71].

as a benchmark since the designs analyzed in the two studies are primarily the same. The system configuration investigated in that work along with the boundary conditions and governing equations was revised using the present simulation model. The cited reference work examined the influence of integrated fins attached to both the internal and external tubes of the PCM shell at uniform wall-temperature conditions. Two performance parameters were applied to evaluate the validity of this model: the PCM's thermal conduct and the liquid fraction's growth. Figure 3 illustrates the outcomes of the validation case, which confirms that the numerical and experimental data of Mat et al. [71] are close to the current model estimates for both the liquid fraction and the average temperature of PCM. A maximum percentage error of less than 2% is reported in this validation test. Thus, the current model can be adopted for examining the thermal characteristics of the PCM-based triple-tube system with a frustum tube.

5. Results and Discussion

A series of numerical simulation tests were conducted based on the mathematical model formulated in the preceding section to evaluate the tube geometry modification on the thermal response of PCM contained in a triplex tube containment design during the mode of the energy charging (melting phase). The tube surface area, which is exposed to the heating effect according to the target phase change method, is enhanced by implementing a single internal frustum tube in a vertical triplex tube system keeping the outer shell unchanged. Frustum tube allows for a more comprehensive modification of the tube geometry over the heat-transfer flow direction, making the approach relevant in more design situations. Gap width, which denotes the radial distance between the inner and middle tubes, was used as the characteristic length of the PCM domain. Different gap widths for the annulus holding the PCM between the middle and inner tubes were investigated as the critical design parameter to explore the benefits of the tube geometry variation along the heat-transfer flow direction. Three scenarios were adopted to investigate the possible thermal response improvement due to the tube geometry modification: Scenario 1: changing the middle tube to a frustum tube; scenario 2: changing the inner tube to a frustum tube; and scenario 3: changing both the inner and middle tube to frustum tubes. In each scenario, as indicated in Figure 1, there are three cases with three different gap widths ($\delta = 5$, 10, and 15 mm) except scenario 2 where only two gap widths ($\delta = 10$ and 15 mm) were used. The effects of modifying the tube geometry and gap width were evaluated by examining the contour lines and the profiles of liquid fraction and average PCM temperature and the melting time and heat storage/recovery rates.

5.1. Liquid-Fraction Evolution. Figure 4 illustrates the liquid-fraction **evolution contours at four different periods of melting (600, 1200, 2400, and 3600 s) for all scenarios, as mentioned earlier. Heat conduction dominates the heat transfer process initially for (t = 600 s). The melting fronts marked in light green appear to be nearly parallel to the tube walls, but there are no significant differences between all cases throughout this period. As time proceeds to (t = 1200 s), a role appears for natural convection, which mainly accelerates the melting rate in the upper zones of the PCM domain. This indicates that warm streams of liquid PCM always tend to be settled at the top since the weight of warm liquid PCM is less than the density of cold solid PCM.

Meanwhile, the melting front movement does not progress much at the bottom, as seen in all cases considered in Figure 4. As time proceeds to (t = 2400 s), the melting fronts show more uniformity in movement through the unsolidified layers of PCM. In contrast, liquid-fraction contours show increasing shrinking in the blue zones, especially in the upper parts. This is because natural convection predominates the melting process over thermal conduction during this period. This drives the melting fronts to show faster

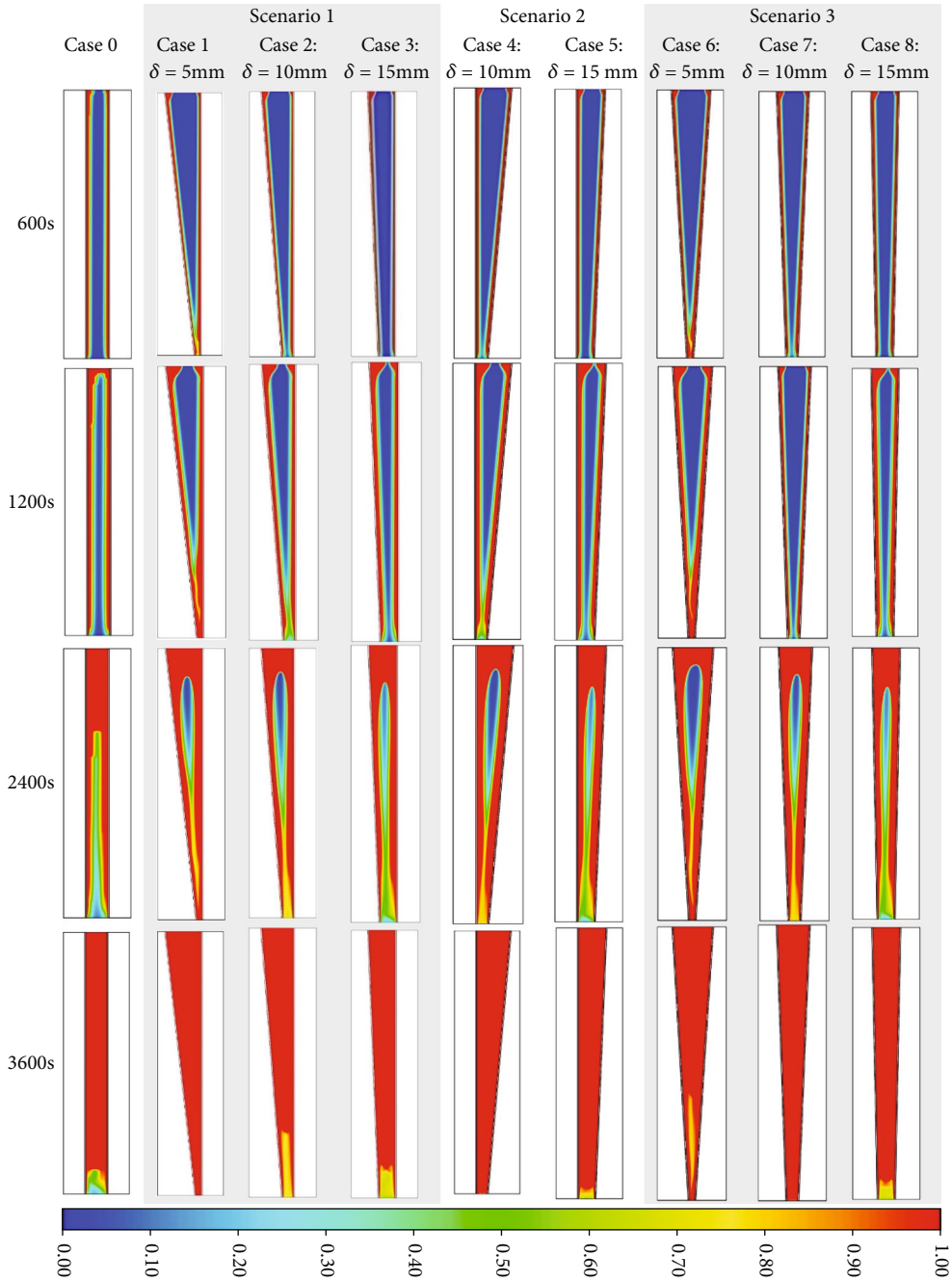

Figure 4: Contours of the liquid-fraction evolution for the investigated tube geometries over various melting times.

movement than in the preceding period. Through the last period (t = 3600 s), even melting is terminated in the upper parts of the domain in all cases; it ultimately terminated in the whole domain only in case 1 ($\delta = 5$ mm) of scenario 1 and case 7 ($\delta = 10$ mm) of scenario 2. The reasons are as follows: (i) the heat exchanging area between HTF and PCM of case 1 is bigger than that of other cases owing to its gap width value (i.e., $\delta = 5$ mm), which is the smallest one used, and (ii) the tilted heating wall from both sides in case 7 gives the melted portions of PCM the potential to move faster and better wash the not yet melted portions as the tilted heating wall can provide a better buoyancy effect than a vertical heating wall. Therefore, these findings suggest that applying a smaller gap width leads to a higher tilt angle of the heating walls, which provides a better potential for more vigorous washing action at the melting fronts.

5.2. Velocity Field. Figure 5 provides a visual representation of the velocity field for all cases within the three scenarios considered for the tube geometry modification and over various melting periods (600, 1200, 2400, and 3600 s). Through the early period ($t \leq 600\,s$), the major PCM domain experienced no movement of liquid PCM as the major PCM has not melted yet. Therefore, the velocity contours are almost

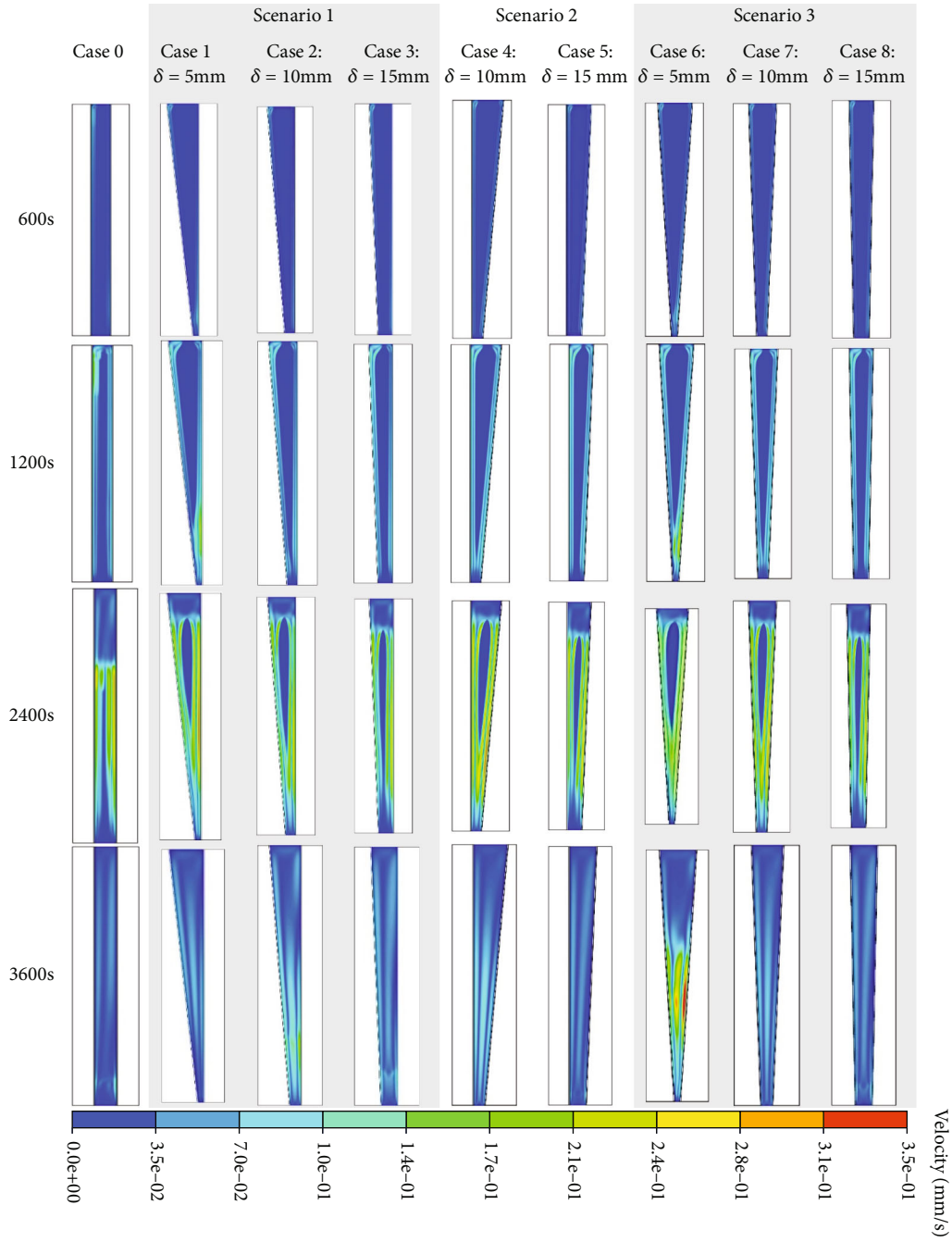

Figure 5: Contours of the velocity field for the investigated tube geometries over various melting times.

identical and marked by blue as a sign of zero velocities. Though this scenario is thermally unstable, the mode of heat transfer is soon altered to contribute from natural convection and conduction during the second period ($600 < t \leq 1200$ s). This period also witnesses the appearance of velocity boundary layers adjacent to the heating walls. However, the values of velocities remain relatively low within the order of 1×10^{-1} mm/s. Furthermore, modifying the tube geometry into frustum results in minor changes in flow velocity over the aforementioned periods. As moving to the next period, the convection movement becomes stronger and more effective at higher portions of the annulus, where the convection rotating part start to expand from below, moving warm liquid to the upper part, while cold liquid with relatively high densities remains trapped below, allowing the melting rate to increase more rapidly in this region. Also explained by this is the production of comparatively high velocities at the top of the domain, which progressively decreases as the rotating cell moves lower, as shown in Figure 5 ($t = 2400$ s). The velocity field appears to show faster movement as the blue color of the velocity field turns red with relatively big rotating cells at the top half of the domain during the final period ($t = 3600$ s). The modification of tube geometry as that in case 1 helps the better

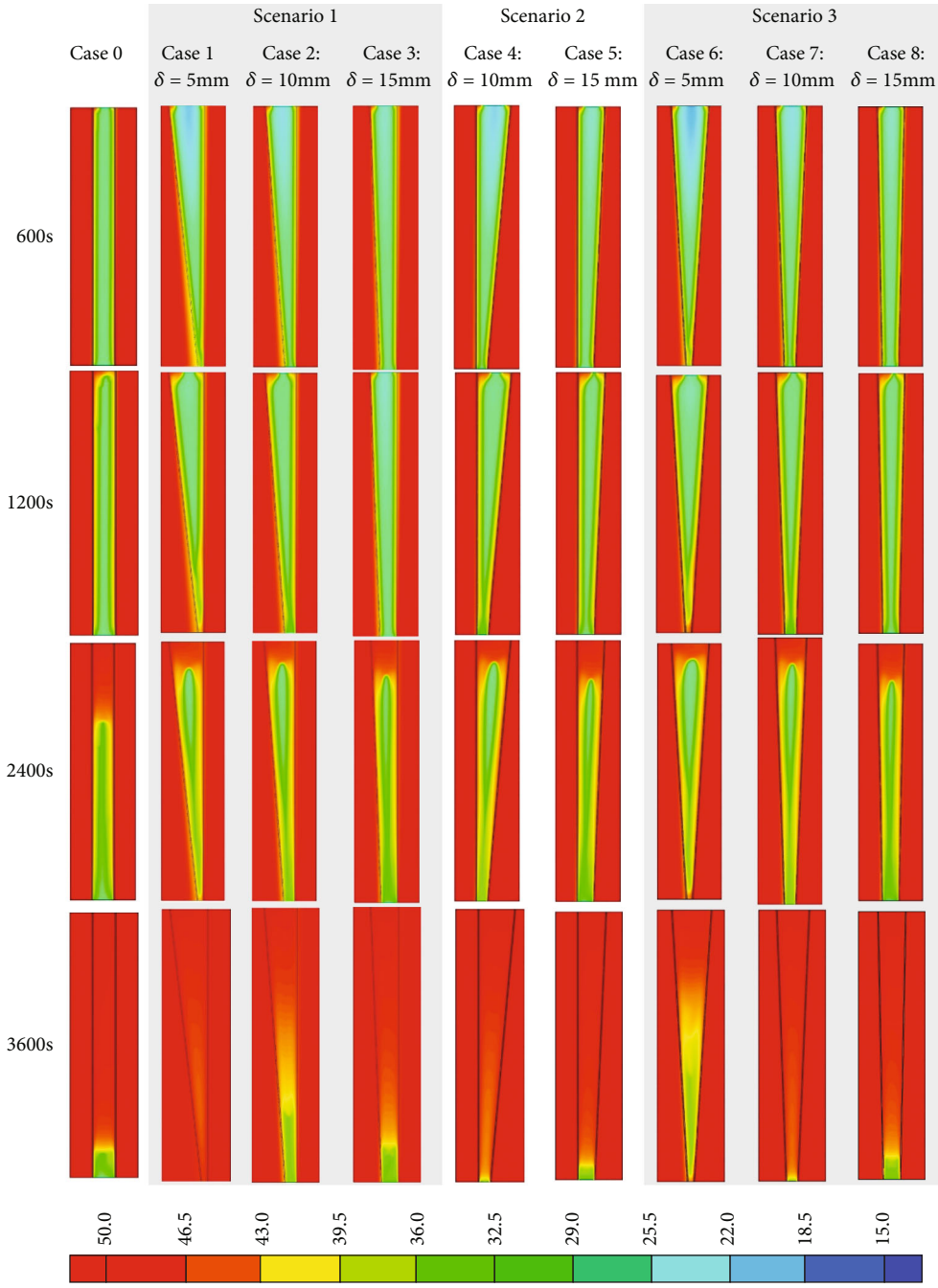

Figure 6: Contours of the temperature distribution for the investigated tube geometries over various melting times.

movement of buoyancy-driven flow, which results in a further increase in flow velocity over the final melting stages. This is expected as the modification of tube geometry into the frustum, especially in cases 1 and 7, helps the formation of bigger rotating cells compared to other cases due to the good role of natural convection, which empowers a substantial propagation of melting as earlier indicated in discussing the dynamic behavior of melting front movement.

5.3. Temperature Distribution. In Figure 6, the isotherm distribution contours for all cases in the discussion and over different melting periods (600, 1200, 2400, and 3600 s) for the studied scenarios of tube geometry modification are given. During the initial stages (t = 600 and 1200 s), the inhomogeneity of local natural convection across the different parts of the PCM domain triggers the PCM temperature to be higher at the bottom than the temperature at the top or center of the PCM domain in all studied cases except case 1. This implies that case 1 has a higher temperature gradient in the gravity direction than other cases, which is advantageous for developing natural convection during the later periods. During the third period (t = 2400 s), the isotherms almost have a similar appearance to each other, and some recirculation cells started to appear near the center of the PCM

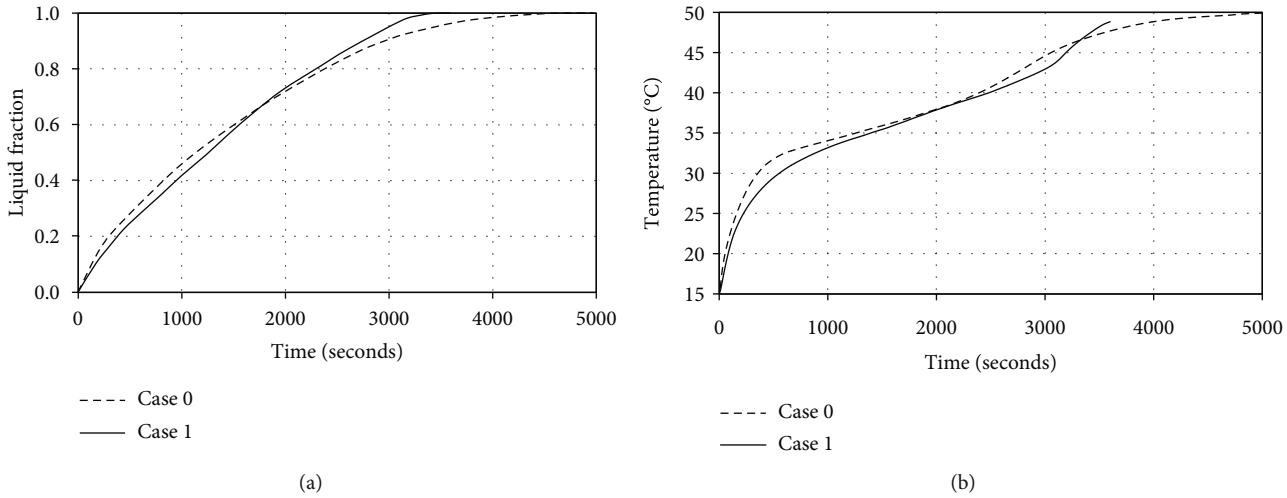

Figure 7: The time-wise variation of (a) liquid-fraction and (b) average temperature for the PCM melting for cases 0 and 1.

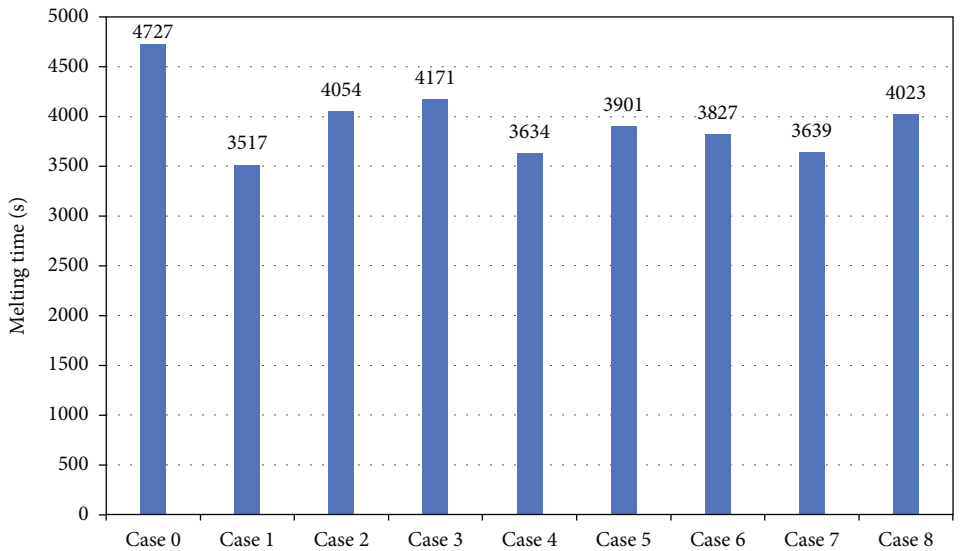

Figure 8: The melting time required for the melting completion for different tube configurations.

domain, especially in the upper half of the domain. This is because the buoyancy effect which originates from the temperature gradient in the vertical direction, outweighs the gravity impact, and triggers the melted portions of PCM to flow, resulting in the formation of recirculation cells. Therefore, natural convection has a greater impact on the temperature field than conduction does during this time. This confirms that during this period, modifying the tube geometry into frustum further enhances the heat transfer by natural convection between the liquid PCM and the HTF during the melting mode. For frustum tubes, a bigger one with smaller gap width such as that in case 1 helps faster heat diffusion across the PCM domain so that the whole PCM reaches the highest temperature in the range, marked in red at t = 3600 s. This indicates that the strength of natural convection further improves as the gap width between the frustum tubes decreases.

5.4. Melting Behavior Profiles. As the best performing among the eight cases of frustum tubes, case 1, which involves Changing the middle tube to a frustum tube with the gap width ($\delta = 5$ mm), is selected to compare the effect of employing frustum tubes over the straight tubes on melting behavior of PCM in a triplex tube storage system. The time histories for liquid-fraction profile and average temperature behavior for cases, case 0 (straight tubes) and case 1 (frustum tube), are compared in Figures 7(a) and 7(b), respectively. As seen in the figure, modifying the tube geometry does not significantly improve the PCM liquid-fraction profile or average temperature behavior at the early durations of melting (i.e., for $t \leq 2400$ s). However, as time advances, it can be observed that employing frustum tubes in case 1 typically provides better heat transfer into the PCM due to the larger heat-exchanging area with the HTF than in the base (case 0). This allows the PCM in case 1 to terminate melting

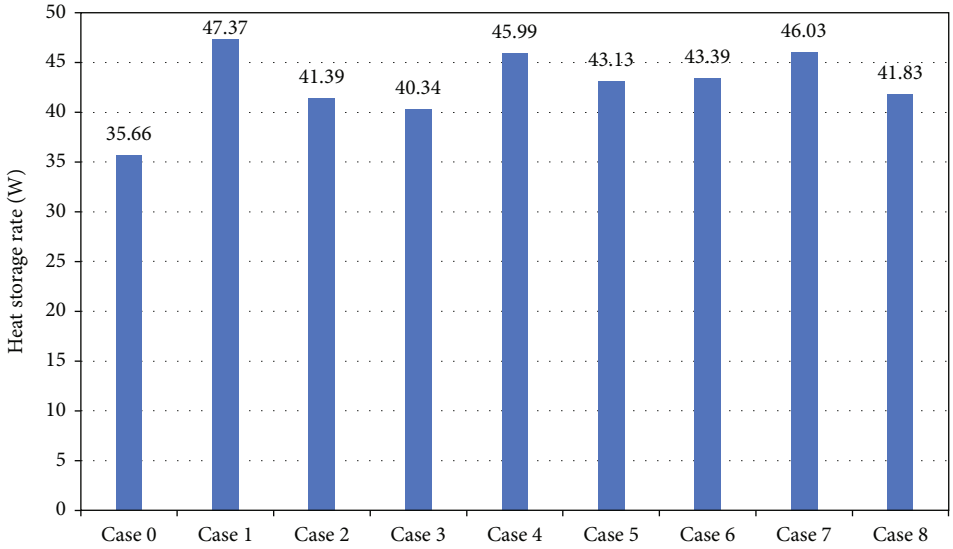

Figure 9: The heat storage rate during melting mode for different tube configurations.

within 3500 s of operation while case 0 needed about 5000 s to complete melting. Moreover, the whole PCM in case 1 reaches the melting temperature (Tl = 49°C) in Figure 7(b) faster than that in case 0 by about 600 s. The reason is that the heat transport from HTF to the PCM during the early periods via conduction is later stored as sensible heat in the residual parts of PCM, leading to a rapid increase in the PCM average temperature during the final periods. The other reason is that the geometry of the frustum tube in case 1 enables a better dominating role of natural convection during the final periods. It should be noted that natural convection in such a situation could serve as a further supply of heat transport into PCM, helping the average temperature of PCM to reach its maximum value in a shorter melting duration in case 1. In fact, the higher the average temperature of PCM, the faster the melting rate and the better the thermal storage process in the PCM-based energy storage system.

5.5. Heat Storage Rates. Figures 8 and 9 show the values of melting time and heat storage rate for each of the cases under discussion. Data from Figure 8 indicates that the time needed to melt the PCM completely is 4727, 3517, 4054, 4171, 3634, 3901, 3827, 3639, and 4023 seconds for cases 0, 1, 2, 3, 4, 5, 6, 7, and 8, respectively. By using case 0 as a referential case to compare with, the results reveal that the melting time could be reduced by 25.6, 14.2, 11.8, 23.1, 17.5, 19.0, 23.0, and 14.9% for cases 1, 2, 3, 4, 5, 6, 7, and 8, respectively. Thus, altering the geometry of the triplex tubes into frustum significantly improves the energy storage process during the melting mode. As a result, all frustum tube systems have shorter melting times than the straight tube system. Furthermore, data from Figure 9 indicates that the heat added to the PCM during the melting mode can be stored at the rate of 35.66, 47.37, 41.39, 40.34, 45.99, 43.13, 43.39, 46.03, and 41.83 watts for cases 0, 1, 2, 3, 4, 5, 6, 7, and 8, respectively. Therefore, when compared to case 0, the heat storage rate could be increased by 32.8, 16.1, 13.1, 29.0, 21.0, 21.7, 29.1, and 17.3% for cases 1, 2, 3 4, 5, 6, 7, and 8, respectively. As a result, heat storage rates are increased for all frustum tube systems compared to straight tube systems. To sum up, data from Figures 8 and 9 also indicates that case 1 performs the best, reducing 25.6% of melting time and increasing the heat storage rate by 32.8%. This suggests that among the tested cases, changing the geometry of the central tube to a frustum and employing a smaller gap width ($\delta = 5$ mm) has the most potential for improving the PCM thermal response during the melting mode.

6. Conclusions

Numerical analyses of the melting process are performed to evaluate the effects of the configuration modification on the thermal response of the PCM contained in a triplex tube storage system. The model is investigated in a three-dimensional configuration via commercial software (ANSYS-FLUENT). To enhance the heating and cooling processes in the system, the surface area of the tube is treated by single or multi-internal frustum tubes in vertical triplex tubes, including the ordinary straight triplex tubes. There are eight cases prepared in this work based on three scenarios: scenario 1: changing the middle tube to a frustum tube; scenario 2: changing the inner tube to a frustum tube; and scenario 3: changing both the inner and middle tube to frustum tubes. The cases were evaluated considering the charging duration and the heat storage rates. The main conclusions can be summarized as follows:

(1) Heat storage rates for all frustum tube systems are higher than those for straight tube systems. Because of the small gap width of case 1, which makes the surface area between heat transfer fluid and PCM bigger than that of other cases, case 1 was found to be the optimal case for the melting time-saving potential and the overall heat storage rate

(2) Using smaller values for the gap width between the tubes currying the heat-transfer fluid (HTF) increases the heat-exchanging areas between the PCM and HTF in charge. Therefore, the frustum tube configurations with smaller gap widths have a better potential for enhancing the PCM thermal response during the melting process

(3) In comparison to the straight tube configuration, the total melting times could be saved by 25.6, 14.2, 11.8, 23.1, 17.5, 19.0, 23.0, and 14.9% for the studied cases from 1 to 8, respectively. The results also indicate that the heat storage rate for the same studied cases could be raised by 32.8%, 16.1%, 13.1%, 29.0%, 21.0, 21.7, 29.1%, and 17.3%, respectively

Data Availability

Data will be provided on request.

Conflicts of Interest

The authors declare that they have no conflicts of interest.

References

[1] B. Ji, F. Zhang, X. Song, and Y. Tang, "A novel potassium-ion-based dual-ion battery," *Advanced Materials*, vol. 29, no. 19, p. 1700519, 2017.

[2] H. Xu, T. He, N. Zhong, B. Zhao, and Z. Liu, "Transient thermomechanical analysis of micro cylindrical asperity sliding contact of SnSbCu alloy," *Tribology International*, vol. 167, article 107362, 2022.

[3] M. S. Mahdi, H. B. Mahood, A. A. Khadom, A. N. Campbell, M. Hasan, and A. O. Sharif, "Experimental investigation of the thermal performance of a helical coil latent heat thermal energy storage for solar energy applications," *Thermal Science and Engineering Progress*, vol. 10, pp. 287–298, 2019.

[4] M. Wang, C. Jiang, S. Zhang, X. Song, Y. Tang, and H.-M. Cheng, "Reversible calcium alloying enables a practical room-temperature rechargeable calcium-ion battery with a high discharge voltage," *Nature Chemistry*, vol. 10, no. 6, pp. 667–672, 2018.

[5] X. Zhang, Y. Tang, F. Zhang, and C. S. Lee, "A novel aluminum–graphite dual-ion battery," *Advanced energy materials*, vol. 6, no. 11, p. 1502588, 2016.

[6] S. Mu, Q. Liu, P. Kidkhunthod, X. Zhou, W. Wang, and Y. Tang, "Molecular grafting towards high-fraction active nanodots implanted in N-doped carbon for sodium dual-ion batteries," *National science review*, vol. 8, no. 7, p. nwaa178, 2020.

[7] W. Qiao, W. Liu, and E. Liu, "A combination model based on wavelet transform for predicting the difference between monthly natural gas production and consumption of US," *Energy*, vol. 235, article 121216, 2021.

[8] M. S. Mahdi, H. B. Mahood, A. A. Khadom, and A. N. Campbell, "Numerical simulations and experimental verification of the thermal performance of phase change materials in a tube-bundle latent heat thermal energy storage system," *Applied Thermal Engineering*, vol. 194, article 117079, 2021.

[9] P. Yang, H. D. Ng, and H. Teng, "Numerical study of wedge-induced oblique detonations in unsteady flow," *Journal of Fluid Mechanics*, vol. 876, pp. 264–287, 2019.

[10] W. Qiao, Y. Wang, J. Zhang, W. Tian, Y. Tian, and Q. Yang, "An innovative coupled model in view of wavelet transform for predicting short- term PM10 concentration," *Journal of Environmental Management*, vol. 289, article 112438, 2021.

[11] H. Wu, X. Hu, X. Li et al., "Large-scale fabrication of flexible EPDM/MXene/PW phase change composites with excellent light-to-thermal conversion efficiency via water-assisted melt blending," *Composites Part A: Applied Science and Manufacturing*, vol. 152, article 106713, 2022.

[12] J. He, P. Xu, R. Zhou et al., "Combustion synthesized electrospun InZnO nanowires for ultraviolet photodetectors," *Advanced Electronic Materials*, vol. 8, no. 4, p. 2100997, 2022.

[13] P. Talebizadehsardari, J. M. Mahdi, H. I. Mohammed, M. Moghimi, A. H. Eisapour, and M. Ghalambaz, "Consecutive charging and discharging of a PCM-based plate heat exchanger with zigzag configuration," *Applied Thermal Engineering*, vol. 193, article 116970, 2021.

[14] R. B. Mahani, H. I. Mohammed, J. M. Mahdi et al., "Phase change process in a zigzag plate latent heat storage system during melting and solidification," *Molecules*, vol. 25, no. 20, p. 4643, 2020.

[15] M. Ghalambaz, H. I. Mohammed, A. Naghizadeh et al., "Optimum placement of heating tubes in a multi-tube latent heat thermal energy storage," *Materials*, vol. 14, no. 5, p. 1232, 2021.

[16] X. Sun, H. I. Mohammed, M. E. Tiji et al., "Investigation of heat transfer enhancement in a triple TUBE latent heat storage system using circular fins with inline and staggered arrangements," *Nanomaterials*, vol. 11, no. 10, p. 2647, 2021.

[17] Y. Ju, T. Zhu, R. Mashayekhi et al., "Evaluation of multiple semi-twisted tape inserts in a heat exchanger pipe using Al2O3 nanofluid," *Nanomaterials*, vol. 11, no. 6, p. 1570, 2021.

[18] M. Yang, C. Li, L. Luo, R. Li, and Y. Long, "Predictive model of convective heat transfer coefficient in bone micro- grinding using nanofluid aerosol cooling," *International Communications in Heat and Mass Transfer*, vol. 125, article 105317, 2021.

[19] X. Liu, H. I. Mohammed, A. Z. Ashkezari, A. Shahsavar, A. K. Hussein, and S. Rostami, "An experimental investigation on the rheological behavior of nanofluids made by suspending multi-walled carbon nanotubes in liquid paraffin," *Journal of Molecular Liquids*, vol. 300, article 112269, 2020.

[20] A. D. Farahani, S. D. Farahani, and E. Hajian, "Efficacy of magnetic field on nanoparticle-enhanced phase change material melting in a triple tube with porous fin," *Heat Transfer Research*, vol. 52, no. 12, 2021.

[21] R. D. C. Oliveski, F. Becker, L. A. O. Rocha, C. Biserni, and G. E. S. Eberhardt, "Design of fin structures for phase change material (PCM) melting process in rectangular cavities," *Journal of Energy Storage*, vol. 35, article 102337, 2021.

[22] A. Chamkha, A. Doostanidezfuli, E. Izadpanahi, and M. Ghalambaz, "Phase-change heat transfer of single/hybrid nanoparticles-enhanced phase- change materials over a heated horizontal cylinder confined in a square cavity," *Advanced Powder Technology*, vol. 28, no. 2, pp. 385–397, 2017.

[23] Y. Zhang, C. Li, D. Jia, D. Zhang, and X. Zhang, "Experimental evaluation of the lubrication performance of MoS_2/CNT nanofluid for minimal quantity lubrication in Ni-based alloy

grinding," *International Journal of Machine Tools and Manufacture*, vol. 99, pp. 19–33, 2015.

[24] N. S. Bondareva, M. Ghalambaz, and M. A. Sheremet, "Influence of the fin shape on heat transport in phase change material heat sink with constant heat loads," *Energies*, vol. 14, no. 5, p. 1389, 2021.

[25] A. Kumar, R. Kothari, S. K. Sahu, S. I. Kundalwal, and M. P. Paulraj, "Numerical investigation of cross plate fin heat sink integrated with phase change material for cooling application of portable electronic devices," *International Journal of Energy Research*, vol. 45, no. 6, pp. 8666–8683, 2021.

[26] S. Tuly, M. Rahman, M. Sarker, and R. Beg, "Combined influence of fin, phase change material, wick, and external condenser on the thermal performance of a double slope solar still," *Journal of Cleaner Production*, vol. 287, article 125458, 2021.

[27] P. Talebizadeh Sardari, H. I. Mohammed, J. M. Mahdi et al., "Localized heating element distribution in composite metal foam-phase change material: Fourier's law and creeping flow effects," *International Journal of Energy Research*, vol. 45, no. 9, pp. 13380–13396, 2021.

[28] C. Nie, J. Liu, and S. Deng, "Effect of geometry modification on the thermal response of composite metal foam/phase change material for thermal energy storage," *International Journal of Heat and Mass Transfer*, vol. 165, article 120652, 2021.

[29] J. Duan and F. Li, "Transient heat transfer analysis of phase change material melting in metal foam by experimental study and artificial neural network," *Journal of Energy Storage*, vol. 33, article 102160, 2021.

[30] M.-R. Wang, L. Deng, G.-C. Liu et al., "Porous organic polymer-derived nanopalladium catalysts for chemoselective synthesis of antitumor benzofuro [2, 3-b] pyrazine from 2-bromophenol and isonitriles," *Organic Letters*, vol. 21, no. 13, pp. 4929–4932, 2019.

[31] H. Teng, H. D. Ng, K. Li, C. Luo, and Z. Jiang, "Evolution of cellular structures on oblique detonation surfaces," *Combustion and Flame*, vol. 162, no. 2, pp. 470–477, 2015.

[32] M. S. Mahdi, H. B. Mahood, A. A. Alammar, and A. A. Khadom, "Numerical investigation of PCM melting using different tube configurations in a shell and tube latent heat thermal storage unit," *Thermal Science and Engineering Progress*, vol. 25, article 101030, 2021.

[33] B. Debich, A. El Hami, A. Yaich, W. Gafsi, L. Walha, and M. Haddar, "Design optimization of PCM-based finned heat sinks for mechatronic components: a numerical investigation and parametric study," *Journal of Energy Storage*, vol. 32, article 101960, 2020.

[34] M. Ghalambaz, S. M. H. Zadeh, S. Mehryan, I. Pop, and D. Wen, "Analysis of melting behavior of PCMs in a cavity subject to a non-uniform magnetic field using a moving grid technique," *Applied Mathematical Modelling*, vol. 77, pp. 1936–1953, 2020.

[35] S. Mehryan, M. Vaezi, M. Sheremet, and M. Ghalambaz, "Melting heat transfer of power-law non-Newtonian phase change nano-enhanced n-octadecane-mesoporous silica ($MPSiO_2$)," *International Journal of Heat and Mass Transfer*, vol. 151, article 119385, 2020.

[36] W. Qiao, Z. Li, W. Liu, and E. Liu, "Fastest-growing source prediction of US electricity production based on a novel hybrid model using wavelet transform," *International Journal of Energy Research*, vol. 46, no. 2, pp. 1766–1788, 2022.

[37] Y. Zhang, C. Li, D. Jia, D. Zhang, and X. Zhang, "Experimental evaluation of MoS_2 nanoparticles in jet MQL grinding with different types of vegetable oil as base oil," *Journal of Cleaner Production*, vol. 87, pp. 930–940, 2015.

[38] T. Gao, C. Li, Y. Zhang et al., "Dispersing mechanism and tribological performance of vegetable oil-based CNT nanofluids with different surfactants," *Tribology International*, vol. 131, pp. 51–63, 2019.

[39] S. H. Park, Y. G. Park, and M. Y. Ha, "A numerical study on the effect of the number and arrangement of tubes on the melting performance of phase change material in a multi-tube latent thermal energy storage system," *Journal of Energy Storage*, vol. 32, article 101780, 2020.

[40] N. Kousha, M. Rahimi, R. Pakrouh, and R. Bahrampoury, "Experimental investigation of phase change in a multitube heat exchanger," *Journal of Energy Storage*, vol. 23, pp. 292–304, 2019.

[41] P. Talebizadehsardari, H. I. Mohammed, J. M. Mahdi et al., "Effect of airflow channel arrangement on the discharge of a composite metal foam-phase change material heat exchanger," *International Journal of Energy Research*, vol. 45, no. 2, pp. 2593–2609, 2021.

[42] H. I. Mohammed, "Discharge improvement of a phase change material-air-based thermal energy storage unit for space heating applications using metal foams in the air sides," *Heat Transfer*, vol. 51, no. 5, 2002.

[43] M. Trafczynski, M. Markowski, K. Urbaniec, P. Trzcinski, S. Alabrudzinski, and W. Suchecki, "Estimation of thermal effects of fouling growth for application in the scheduling of heat exchangers cleaning," *Applied Thermal Engineering*, vol. 182, article 116103, 2021.

[44] B. Li, C. Li, Y. Zhang et al., "Heat transfer performance of MQL grinding with different nanofluids for Ni- based alloys using vegetable oil," *Journal of Cleaner Production*, vol. 154, pp. 1–11, 2017.

[45] A. Piccolo and A. J. Jaworski, "Experimental study of heat transfer characteristics of finned-tube and circular-pore heat exchangers in oscillatory flow," *Applied Thermal Engineering*, vol. 181, article 116022, 2020.

[46] E. M. El-Said, M. Abdulaziz, and M. M. Awad, "Thermodynamic performance evaluation for helical plate heat exchanger based on second law analysis," *Proc Roman Acad Ser A*, vol. 19, pp. 237–242, 2018.

[47] E. M. El-Said, M. Abdulaziz, and M. M. Awad, ""A numerical investigation on heat transfer enhancement and the flow characteristics in a new type plate heat exchanger using helical flow duct, " cogent," *Engineering*, vol. 4, no. 1, article 1396638, 2017.

[48] T. Gao, C. Li, D. Jia et al., "Surface morphology assessment of CFRP transverse grinding using CNT nanofluid minimum quantity lubrication," *Journal of Cleaner Production*, vol. 277, article 123328, 2020.

[49] A. Pourakabar and A. A. R. Darzi, "Enhancement of phase change rate of PCM in cylindrical thermal energy storage," *Applied Thermal Engineering*, vol. 150, pp. 132–142, 2019.

[50] R. Qaiser, M. M. Khan, L. A. Khan, and M. Irfan, "Melting performance enhancement of PCM based thermal energy storage system using multiple tubes and modified shell designs," *Journal of Energy Storage*, vol. 33, article 102161, 2021.

[51] X. Yang, J. Guo, B. Yang, H. Cheng, P. Wei, and Y.-L. He, "Design of non-uniformly distributed annular fins for a

shell-and-tube thermal energy storage unit," *Applied Energy*, vol. 279, article 115772, 2020.

[52] J. Guo, Z. Du, G. Liu, X. Yang, and M.-J. Li, "Compression effect of metal foam on melting phase change in a shell-and-tube unit," *Applied Thermal Engineering*, vol. 206, article 118124, 2022.

[53] X. Yang, X. Wang, Z. Liu, X. Luo, and J. Yan, "Effect of fin number on the melting phase change in a horizontal finned shell- and-tube thermal energy storage unit," *Solar Energy Materials and Solar Cells*, vol. 236, article 111527, 2022.

[54] J. Guo, X. Wang, B. Yang, X. Yang, and M.-J. Li, "Thermal assessment on solid-liquid energy storage tube packed with non-uniform angled fins," *Solar Energy Materials and Solar Cells*, vol. 236, article 111526, 2022.

[55] J. Guo, Z. Liu, B. Yang, X. Yang, and J. Yan, "Melting assessment on the angled fin design for a novel latent heat thermal energy storage tube," *Renewable Energy*, vol. 183, pp. 406–422, 2022.

[56] A. H. Eisapour, M. Eisapour, H. I. Mohammed, A. Shafaghat, M. Ghalambaz, and P. Talebizadehsardari, "Optimum design of a double elliptical latent heat energy storage system during the melting process," *Journal of Energy Storage*, vol. 44, article 103384, 2021.

[57] H. Ren, M. He, W. Lin, L. Yang, W. Li, and Z. Ma, "Performance investigation and sensitivity analysis of shell-and-tube phase change material thermal energy storage," *Journal of Energy Storage*, vol. 33, article 102040, 2021.

[58] J. R. Patel, M. K. Rathod, R. M. Elavarasan, and Z. Said, "Influence of longitudinal fin arrangement on the melting and solidification inside the triplex tube latent heat thermal storage system," *Journal of Energy Storage*, vol. 46, article 103778, 2022.

[59] J. R. Patel, M. K. Rathod, and M. Sheremet, "Heat transfer augmentation of triplex type latent heat thermal energy storage using combined eccentricity and longitudinal fin," *Journal of Energy Storage*, vol. 50, article 104167, 2022.

[60] M. A. Alnakeeb, M. A. Abdel Salam, and M. A. Hassab, ""Eccentricity optimization of an inner flat-tube double-pipe latent-heat thermal energy storage unit, " case studies," *Thermal Engineering*, vol. 25, article 100969, 2021.

[61] Z.-J. Zheng, Y. Xu, and M.-J. Li, "Eccentricity optimization of a horizontal shell-and-tube latent-heat thermal energy storage unit based on melting and melting-solidifying performance," *Applied Energy*, vol. 220, pp. 447–454, 2018.

[62] Y. Pahamli, M. J. Hosseini, A. A. Ranjbar, and R. Bahrampoury, "Analysis of the effect of eccentricity and operational parameters in PCM- filled single-pass shell and tube heat exchangers," *Renewable Energy*, vol. 97, pp. 344–357, 2016.

[63] M. Faghani, M. J. Hosseini, and R. Bahrampoury, "Numerical simulation of melting between two elliptical cylinders," *Alexandria Engineering Journal*, vol. 57, no. 2, pp. 577–586, 2018.

[64] M. Gorzin, M. J. Hosseini, M. Rahimi, and R. Bahrampoury, "Nano-enhancement of phase change material in a shell and multi-PCM-tube heat exchanger," *Journal of Energy Storage*, vol. 22, pp. 88–97, 2019.

[65] K. Chen, H. I. Mohammed, J. M. Mahdi, A. Rahbari, A. Cairns, and P. Talebizadehsardari, "Effects of non-uniform fin arrangement and size on the thermal response of a vertical latent heat triple-tube heat exchanger," *Journal of Energy Storage*, vol. 45, article 103723, 2022.

[66] F. T. Najim, H. I. Mohammed, H. M. T. Al-Najjar et al., "Improved melting of latent heat storage using fin arrays with non-uniform dimensions and distinct patterns," *Nanomaterials*, vol. 12, no. 3, p. 403, 2022.

[67] P. Talebizadeh Sardari, G. S. Walker, M. Gillott, D. Grant, and D. Giddings, "Numerical modelling of phase change material melting process embedded in porous media: effect of heat storage size," *Proceedings of the Institution of Mechanical Engineers, Part A: Journal of Power and Energy*, vol. 234, no. 3, pp. 365–383, 2020.

[68] J. M. Mahdi and E. C. Nsofor, "Melting enhancement in triplex-tube latent heat energy storage system using nanoparticles-metal foam combination," *Applied Energy*, vol. 191, pp. 22–34, 2017.

[69] M. Esapour, M. Hosseini, A. Ranjbar, Y. Pahamli, and R. Bahrampoury, "Phase change in multi-tube heat exchangers," *Renewable Energy*, vol. 85, pp. 1017–1025, 2016.

[70] W.-B. Ye, D.-S. Zhu, and N. Wang, "Numerical simulation on phase-change thermal storage/release in a plate-fin unit," *Applied Thermal Engineering*, vol. 31, no. 17-18, pp. 3871–3884, 2011.

[71] S. Mat, A. A. Al-Abidi, K. Sopian, M. Y. Sulaiman, and A. T. Mohammad, "Enhance heat transfer for PCM melting in triplex tube with internal-external fins," *Energy Conversion and Management*, vol. 74, pp. 223–236, 2013.

[72] J. M. Mahdi and E. C. Nsofor, "Solidification enhancement in a triplex-tube latent heat energy storage system using nanoparticles-metal foam combination," *Energy*, vol. 126, pp. 501–512, 2017.